Radiation transfer in cylindrical, toroidal and hemi-ellipsoidal plasmas

G. Pérez-Callejo[a,*], J. S. Wark[a], S. J. Rose[a,b]

[a] *Department of Physics, Clarendon Laboratory, University of Oxford, Parks Road, Oxford OX1 3PU, UK*
[b] *Plasma Physics Group, The Blackett Laboratory, Imperial College London, Prince Consort Road, London, SW7 2AZ, UK*

Abstract

We present solutions of the radiative transfer equation for cylinders, hollow hemi-ellipsoidal shells and tori for a uniform plasma of fixed geometry. The radiative transfer equation is explicitly solved for two directions of emission, parallel and perpendicular to the axis of symmetry. The ratio between the fluxes in these two directions is also calculated and its use in measuring the frequency resolved opacity of the plasma is discussed. We find that the optimal geometry to use this ratio as an opacity measurement is a planar geometry.

Keywords: Radiative transfer, Opacity, Spectroscopy, Geometry

1. Introduction

Patch (1971) proposed a method to measure an inverse weighted opacity by integrating the plasma transmissivity over a number of different path lengths [1]. This method has, to our knowledge, never been used experimentally. Preston *et al.* [2], measured the K-shell emission of solid density magnesium by fitting the self-emission of planar targets to the solution of the radiative transfer equation. In their experiment, several targets with different thicknesses were used to obtain different path lengths, and in this way, information of the opacity of the target was obtained.

*Corresponding author: gabriel.perezcallejo@physics.ox.ac.uk

However, it is possible to elliminate the need for using several targets, by taking into account the geometry of the source. Bhatia and coworkers [3, 4, 5] showed that the intensity of optically thick lines can in some cases be enhanced with respect to their optically thin limit. Kerr *et al.* showed that this effect was related to the ratio between the mean chord of the plasma and the Line Of Sight (LOS) through the plasma to the detector [6, 7, 8]. Therefore the relative intensity of lines in spectra will depend on the position of the detector with respect to the source. This effect has been widely studied in astrophysics and several approaches to characterize the geometry of astrophysical plasmas have been proposed [7, 9].

This effect is also present in High Energy Density (HED) experiments [10, 11] with the advantage that, contrary to most astrophysical cases, several LOS can be observed at once. In this way, the differences in spectra from all LOS can be linked to the optical depth, and from it, several plasma properties can be studied. An experimental approach to this method which relies on keeping the plasma geometry constant was previously suggessted by Mancini *et al.* [12].

We present a method to potentially measure the opacity of a plasma from its self-emission using two perpendicular LOS, namely, down the symmetry axis, or Face-on and perpendicular to it, or Side-on. We asume a uniform steady-state plasma whose geometry is constant in time. The method is presented for cylinders, hollow hemi-ellipsoidal shells and plasma tori. The optimal case for obtaining the most accurate opacity measurements using the Face-on and Side-on emission is obtained for a planar geometry (cylinder, or planar ellipsoid).

2. Radiative transfer

As mentioned in the previous section, we assume a steady-state uniform plasma. The one-dimensional radiative transfer equation then has the form

$$\frac{\partial I(\nu, z)}{\partial z} = \eta(\nu) - \kappa(\nu) I(\nu, z), \tag{1}$$

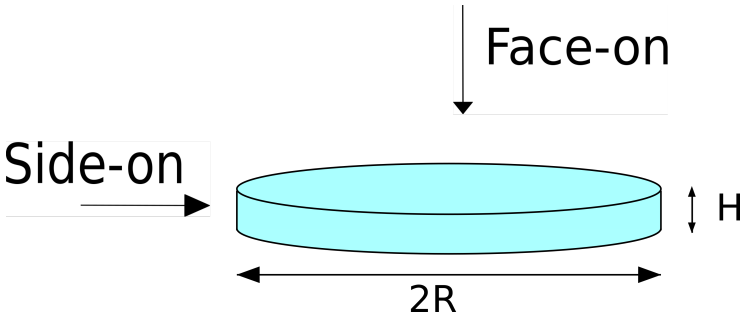

Figure 1: Schematic drawing of a plasma cylinder. The radius is denoted R. The thickness of the shell is H.

which, for a plasma with no external illumination, has the following solution

$$I(\nu, z) = \frac{\eta(\nu)}{\kappa(\nu)} \left(1 - e^{-\kappa(\nu)z}\right) = S(\nu) \left(1 - e^{-\kappa(\nu)z}\right), \tag{2}$$

where $S(\nu)$ is the source function.

However, in practical situations, a detector will measure the emitted flux, not the intensity. Under the assumption that the detector is looking directly at the plasma and sufficiently far from the source, so that all the rays reaching it are parallel, the flux is defined by

$$F(\nu, z) = \frac{1}{d^2} \int I(\nu, z) dA, \tag{3}$$

where A is the projected area seen by the detector and d is the distance from the detector to the source.

3. Plasma cylinder

We will start with the simple case of a uniform plasma cylinder, which has been discussed in depth in reference [13]. Figure 1 shows a schematic drawing of this geometry. We denote the thickness of the cylinder as H and its radius as R.

From equation 3, the flux emitted in the axial direction (Face-on) is

$$F_{fo}(\nu) = \frac{1}{d^2} \int S(\nu) \left(1 - e^{-\kappa(\nu)H}\right) dA, \tag{4}$$

given that the thickness of the plasma is constant and equal to H in the axial direction. Integrating over the projected Face-on surface, the total Face-on flux is

$$F_{fo}(\nu) = \frac{\pi R^2}{d^2} S(\nu) \left(1 - e^{-\kappa(\nu)H}\right). \tag{5}$$

For the Side-on emission the path length and the projected surface depend on the polar angle ϕ. With this angle defined as in reference [13], this dependence is

$$l(\phi) = 2R\sin(\phi), \tag{6}$$

$$dA(\phi) = HR\sin(\phi)d\phi. \tag{7}$$

with ϕ goes from 0 to π. The Side-on flux is then calculated as

$$F_{so}(\nu) = \frac{HR}{d^2} S(\nu) \int_0^{\pi} (1 - e^{-2\kappa(\nu)R\sin(\phi)})\sin(\phi)d\phi, \tag{8}$$

which has the following exact solution

$$F_{so}(\nu) = \frac{2HR}{d^2} S(\nu) \left[1 - \frac{\pi}{2}\left(L_{-1}(2\kappa(\nu)R) - I_1(2\kappa(\nu)R)\right)\right], \tag{9}$$

where L_n is the modified Struve function of order n and I_n is the n-th order modified Bessel function of the first kind [14]. Following Pérez-Callejo *et al.* [13] the term in square brackets in equation 9 can be approximated by the function $1 - e^{-1.45\kappa(\nu)R}$ with an error of less than 5%, thus yielding

$$F_{so}(\nu) = \frac{2HR}{d^2} S(\nu) \left(1 - e^{-1.45\kappa(\nu)R}\right). \tag{10}$$

To simplify the notation we introduce the aspect ratio of the cylinder, $a = H/R$, and the optical depth parameter $\gamma(\nu) = \kappa(\nu)R$. The ratio between the Face-on flux and the Side-on flux can therefore be expressed as

$$\frac{F_{fo}(\nu)}{F_{so}(\nu)} = \frac{\pi}{2a} \cdot \frac{1 - e^{-a\gamma(\nu)}}{1 - e^{-1.45\gamma(\nu)}}. \tag{11}$$

This ratio is shown in figure 2 as a function of $\gamma(\nu)$, where we compare the result from equation 11 with the exact solution (which uses equation 9). To understand the potential use of this expression, consider an experiment in

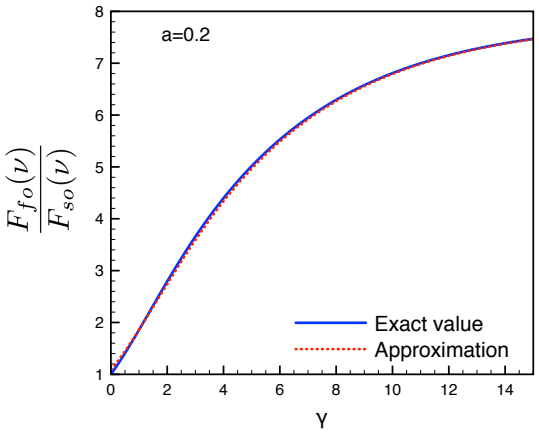

Figure 2: Ratio between the Face-on and Side-on flux for a cylinder (given by equations 5, 9 and 11) as a function of $\gamma(\nu)$. $\gamma(\nu)$ can be obtained from a measurement of this ratio. In the limit of high values of $\gamma(\nu)$ this ratio tends to the ratio between the emitting surface areas in the Face-on and Side-on directions. For optically thin radiation, this ratio is 1, as radiation escapes the plasma isotropically. We show the exact solution (solid line) and the result from the approximation (dotted) for comparison.

which the aspect ratio a is known and the Face-on and Side-on spectra are measured. Equation 11 allows the use of their ratio as a function of frequency to obtain $\gamma(\nu)$, and thereby its frequency dependent opacity ($\gamma(\nu) = \kappa(\nu)R$). The accuracy of the measurement will depend on the limit

$$\frac{F_{fo}/F_{so}(\gamma(\nu) \to \infty)}{F_{fo}/F_{so}(\gamma(\nu) \to 0)} = \frac{1.45}{a}, \tag{12}$$

as when this ratio is greater, the flux ratio is more sensitive to differences in opacity. From equation 12 it follows that in cylindrical geometries, the highest sensitivity with this method is obtained for low aspect ratios.

4. Hemispherical shell

We now consider the case of a hemispherical shell of thickness Δr consisting of a plasma of opacity $\kappa(\nu)$. The hemisphere lies on the XY plane (figure 3). The flux emitted in the z direction (Face-on) is

$$F_{fo}(\nu) = \frac{1}{d^2} \int S(\nu)(1 - e^{-\kappa(\nu)\Delta r'}) dA, \tag{13}$$

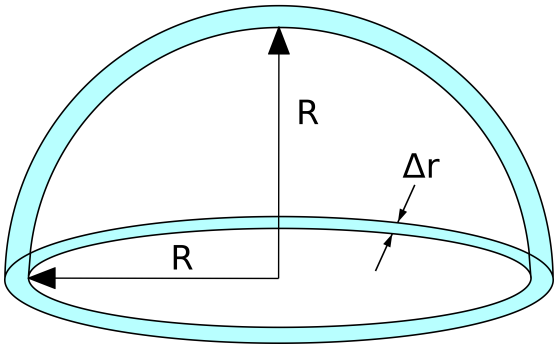

Figure 3: Schematic drawing of a hemispherical shell. The radius is denoted R. The thickness of the shell is Δr.

where $\Delta r'$ is the path traveled in the direction of emission for a given ray. Under the assumption that Δr is small with respect to the radius of the sphere, we take $\Delta r' = \Delta r / \cos(\theta)$, where θ is the polar angle. Defining in this case $\gamma(\nu) = \kappa(\nu)\Delta r$, this equation has the solution

$$F_{fo}(\nu) = \frac{\pi R^2}{d^2} S(\nu) \left[1 - e^{-\gamma(\nu)}(1 - \gamma(\nu)) - \gamma(\nu)^2 E_1(\gamma(\nu))\right] \tag{14}$$

where $E_1(x)$ is the first order exponential integral function [14].

The term in square brackets in equation 14 can be approximated by a function of the form $(1 - e^{-b\gamma(\nu)})$.The value of b that minimizes the difference is 1.5, which yields a maximum error of $\sim 30\%$ for $\gamma(\nu) \to 0$, quickly dropping below 5% for $\gamma(\nu) > 0.45$. A comparison between the exact value and the exponential approximation is shown in figure 4. With this approximation

$$F_{fo}(\nu) = \frac{\pi R^2}{d^2} S(\nu) \left(1 - \exp\left[-1.5\gamma(\nu)\right]\right). \tag{15}$$

The Side-on emission is

$$F_{so}(\nu) = \frac{\pi R^2}{2d^2} S(\nu) \left[1 - e^{-2\gamma(\nu)}(1 - 2\gamma(\nu)) - 4\gamma(\nu)^2 E_1(2\gamma(\nu))\right] \tag{16}$$

Using the same approximation, the Side-on flux is given by

$$F_{so}(\nu) = \frac{\pi R^2}{2d^2} S(\nu) \left(1 - \exp\left[-3\gamma(\nu)\right]\right). \tag{17}$$

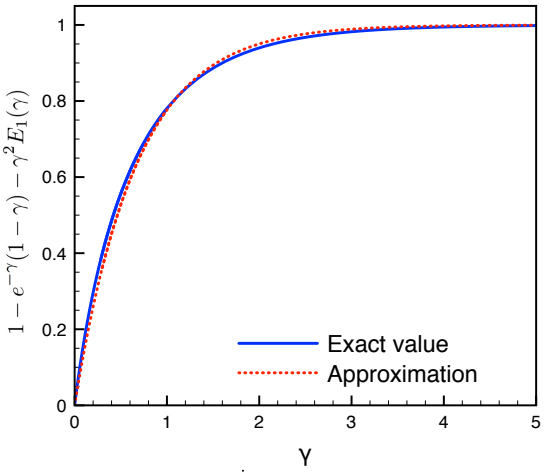

Figure 4: Comparison between the exact value of the square brackets in equation 14 (solid line) and the approximation given in equation 15 (dashed line). The limits in the x-axis have been chosen so that the calculations converge, and the asymptotic behavior can be observed.

The comparison between the flux from both views as a function of $\gamma(\nu) = \kappa(\nu)\Delta r$ is shown in figure 5. For high values of γ this ratio tends asymptotically to 2, which is the ratio between the surface areas seen by the Face-on and Side-on detectors. For optically thin radiation, this ratio is 1, as opacity effects are negligible and radiation escapes the plasma isotropically.

In this particular geometry, the range of the Face-on to Side-on ratio is a factor of 2. Given that this range determines the sensitivity of the opacity measurements obtained from the flux ratio, using a cylinder with $H/R < 0.725$ is preferrable to a spherical shell (see equation 12).

5. Symmetric hemi-ellipsoid

We consider now a symmetric hemi-ellipsoidal shell as shown in figure 6. The thickness of the shell is Δr, and $\gamma(\nu) = \kappa(\nu)\Delta r$ as in the spherical case. The aspect ratio of the ellipsoid is denoted $a = R_2/R_1$. We also assume Δr to be small compared with the two main radii of the hemi-ellipsoid. Proceeding as

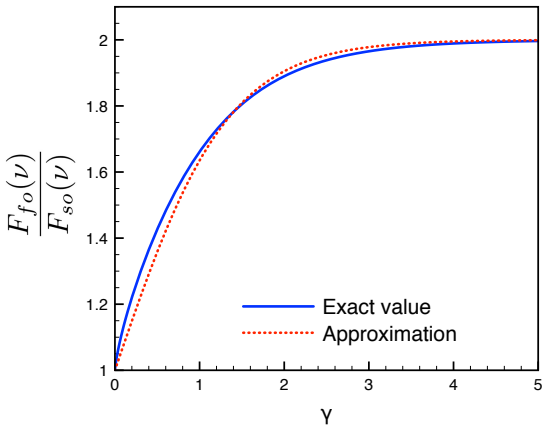

Figure 5: Ratio between the Face-on and Side-on flux for a hemispherical shell as a function of $\gamma(\nu)$. $\gamma(\nu)$ can be obtained from a measurement of this ratio. In the limit of high values of $\gamma(\nu)$ this ratio tends to 2. For optically thin radiation, this ratio is 1, as radiation escapes the plasma isotropically. We show the exact solution, given by equations 14 and 16 (solid line) and the result from the approximation, given by equations 15 and 17 (dotted) for comparison.

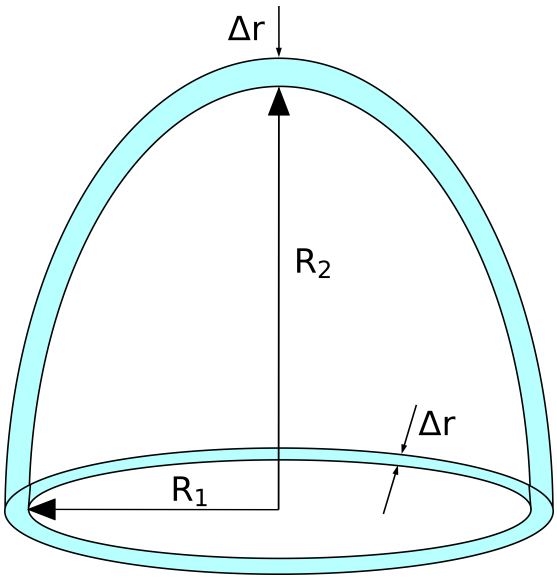

Figure 6: Schematic drawing of a symmetric hemi-ellipsoidal shell. The radius in the basis plane is denoted R_1; the radius in the vertical direction is $R_2 = aR_1$. The thickness of the shell is Δr, as in the previous section.

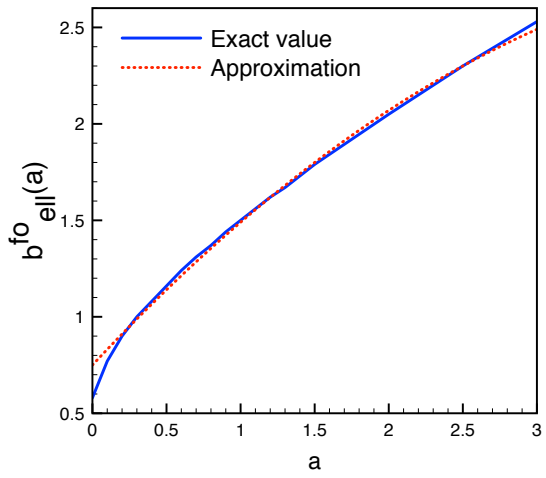

Figure 7: Value of $b^{fo}_{ell}(a)$ such that $1-\exp\left[-b^{fo}_{ell}(a)\gamma\right]$ is the best fit to the exact solution for the Face-on flux of a hemi-ellipsoidal plasma with ratio $R_2/R_1 = a$ (solid line). The dashed line corresponds to a polynomial fit valid for values of a between 0.3 and 3.

in the spherical case, the flux emitted in the Face-on direction is given by

$$F_{fo}(\nu) = \frac{2\pi R_1^2}{d^2} S(\nu) \int_0^{\pi/2} \sin(\theta)\cos(\theta) \left(1 - e^{-\gamma(\nu)\sin(\theta)\left(1+\frac{a}{\tan^2(\theta)}\right)}\right) d\theta, \quad (18)$$

which we will write as

$$F_{fo}(\nu) = \frac{\pi R_1^2}{d^2} S(\nu) G^{fo}_{ell}(a, \gamma(\nu)). \quad (19)$$

where G^{fo}_{ell} asymptotically tends to 1 for high values of $\gamma(\nu)$.

The function G^{fo}_{ell} cannot be expressed as an analytical function, and must be calculated numerically. In a similar way to the previous section, we also approximate it by a function of the form $(1 - \exp[-b^{fo}_{ell}(a)\gamma])$, where here b^{fo}_{ell} depends on a. The values of the function b^{fo}_{ell} that minimise the difference between the true value and the approximation for different values of a, and all γ values are shown in figure 7. A polynomial fit to these values is

$$b^{fo}_{ell}(a) = -0.08a^2 + 0.82a + 0.75. \quad (20)$$

And we approximate the Face-on flux of a symmetric hemi-ellipsoid as

$$F_{fo}(\nu) = \frac{\pi R_1^2}{d^2} S(\nu)(1 - e^{-b^{fo}_{ell}(a)\gamma(\nu)}). \quad (21)$$

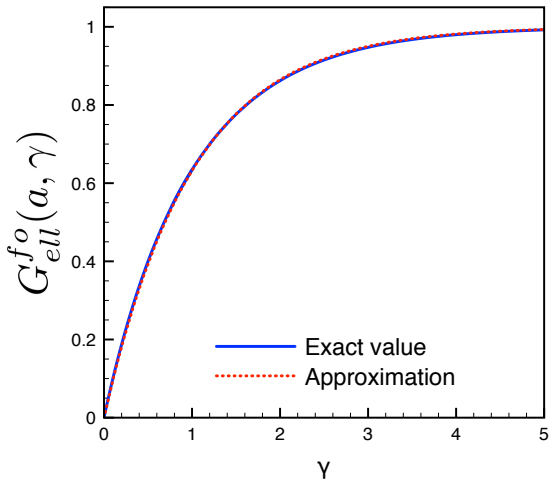

Figure 8: Comparison between the exact value for $G^{fo}_{ell}(a,\gamma)$ (solid line) and the function $1-e^{-b^{fo}_{ell}(a)\gamma}$ (dashed line). The aspect ratio for this example is $a=0.3$.

An example of the comparison between the exact value and the approximation is shown in figure 9. This example corresponds to an aspect ratio $a=0.3$.

The Side-on emission of the hemi-ellipsoid is given by

$$F_{so}(\nu)=\frac{aR_1^2}{d^2}S(\nu)\int_{-\pi/2}^{\pi/2}\cos(\phi)d\phi \int_0^{\pi/2}\cos^2(\theta)\left(1-e^{-2\gamma(\nu)\cos(\theta)/\cos(\phi)\left(1+\frac{\tan^2(\theta)}{a}\right)}\right)d\theta. \quad (22)$$

which we write as

$$F_{so}(\nu)=\frac{\pi aR_1^2}{2d^2}S(\nu)G^{so}_{ell}(a,\gamma(\nu)), \quad (23)$$

where $G^{so}_{ell}(a,\gamma(\nu))$ asymptotically tends to 1 for high values of $\gamma(\nu)$. Using the same approach as previously, equation 23 can be written as

$$F_{so}=\frac{\pi aR_1^2}{2}\cdot\frac{S(\nu)}{d^2}\left(1-e^{-2b^{so}_{ell}(a)\gamma(\nu)}\right). \quad (24)$$

where as before, $b^{so}_{ell}(a)$ is approximated as

$$b^{so}_{ell}(a)=-0.013/a^2+0.298/a+1.191. \quad (25)$$

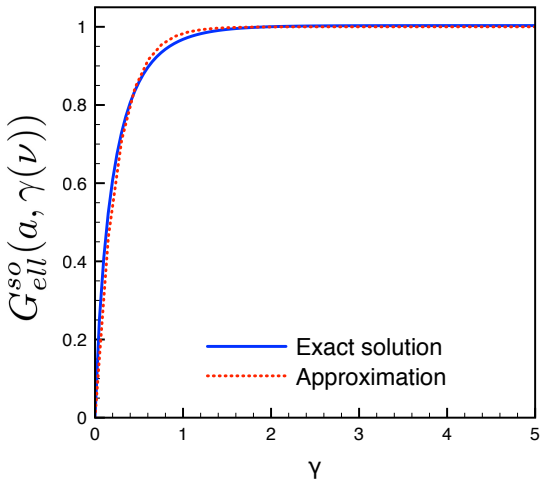

Figure 9: Comparison between the exact value for $G^{so}_{ell}(a,\gamma)$ (solid line) and the function $1-e^{-b^{so}_{ell}(a)\gamma}$ (dashed line). The aspect ratio for this example is $a=0.3$.

The ratio of Face-on to Side-on flux from in a hemi-ellipsoidal shell depends only on $\gamma(\nu)$ and a. As previously discussed, the bigger the range covered by this ratio, that is, the greater the ratio

$$\frac{F_{fo}/F_{so}(a,\gamma(\nu)\to\infty)}{F_{fo}/F_{so}(a,\gamma(\nu)\to 0)} \tag{26}$$

the more precise an opacity measurement will be. This ratio is shown in figure 10, where we show how for small values of a (when the geometry becomes planar), the ratio in equation 26 and therefore the accuracy of an opacity measurement, is seen to be greatest.

6. Torus

The final geometry that we consider is a torus where the radius of revolution is denoted R and the radius of the revolving circle is denoted r. This is schematically shown in figure 11. Here we only consider $R \geq r$.

The Face-on emission (in the direction of the axis) can be considered as the Side-on emission of a series of differential cylinders with thickness $Rd\theta$ and, as

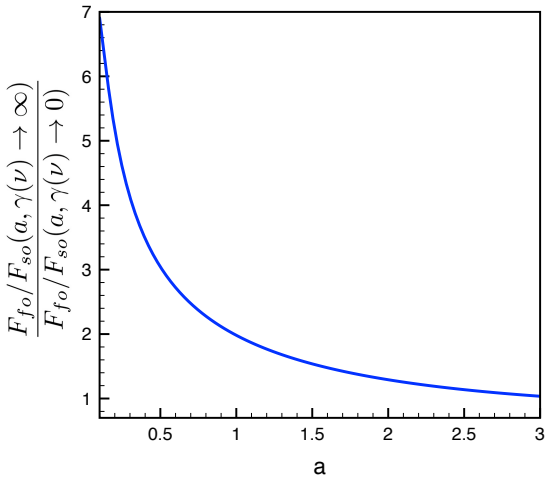

Figure 10: The ratio between the Face-on/Side-on flux for optically thick to optically thin radiation in a symmetric hemi-ellipsoidal plasma as a function of its aspect ratio $a = R_2/R_1$. The greatest sensitivity is obtained for low aspect ratios, that is, when the hemi-ellipsoid becomes planar.

obtained in section 3, has the form [13]

$$F_{fo}(\nu) = \frac{4\pi a r^2}{d^2} S(\nu) \left[1 - \frac{\pi}{2} \left(L_{-1}(2\gamma(\nu)) - I_1(2\gamma(\nu))\right)\right], \tag{27}$$

where for the toroidal geometry, $\gamma(\nu)$ is defined as $\kappa(\nu)r$, and $a = R/r$. So, the Face-on flux of a torus is given to a good approximation by

$$F_{fo} = \frac{4\pi a r^2}{d^2} S(\nu) \left[1 - e^{-1.45\gamma(\nu)}\right]. \tag{28}$$

The Side-on emission of a torus has two different components: rays leaving the torus through its inner hole and then reentering before escaping, and rays that do not go through the hole. The paths that these two different kinds of rays travel are given by

$$\Delta x_h = 2\left[(R + r\sin\phi)\cos(\theta) - \sqrt{(R + r\sin\phi)^2\cos^2(\theta) - 4Rr\sin\phi}\right], \tag{29}$$

and

$$\Delta x_{nh} = 2(R + r\sin\phi)\cos(\theta), \tag{30}$$

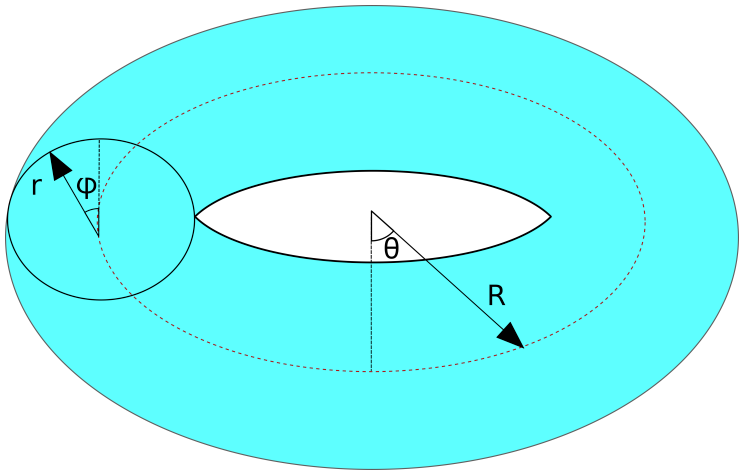

Figure 11: Schematic diagram of a plasma torus. r is the radius of the revolving circle, and R is the revolving radius. The azimuthal and polar angles ϕ and θ are defined as shown.

where Δx_h corresponds to rays that go through the central hole and Δx_{nh} corresponds to rays that do not. The total Side-on flux is the sum of these two contributions, which is

$$F_{so}(\nu) = \frac{4r^2}{d^2} S(\nu) \left[\int_0^{\pi/2} (a + \sin\phi) \sin\phi d\phi \right.$$
$$\left(\int_0^{\arcsin\left(\frac{a-\sin\phi}{a+\sin\phi}\right)} \left[1 - e^{-2\gamma(\nu)\left[(a+\sin\phi)\cos\theta - \sqrt{(a+\sin\phi)^2\cos^2\theta - 4a\sin\phi}\right]} \right] \cos\theta d\theta + \right.$$
$$\left. \left. \int_{\arcsin\left(\frac{a-\sin\phi}{a+\sin\phi}\right)}^{\pi/2} \left[1 - e^{-2\gamma(\nu)(a+\sin\phi)\cos\theta} \right] \cos\theta d\theta \right) \right], \quad (31)$$

which we write as

$$F_{so}(\nu) = \frac{(4a + \pi)r^2}{d^2} S(\nu) G^{so}_{tor}(a, \gamma(\nu)). \quad (32)$$

where G^{so}_{tor} asymptotically tends to 1 for high values of $\gamma(\nu)$.

The function G^{so}_{tor} can be approximated as $(1 - \exp[-b_{tor}(a)\gamma])$ (where $\gamma = \kappa r$). The values of $b_{tor}(a)$ that best fit the exact solution for different aspect ratios is shown in figure 12 together with a fit given by

$$b_{tor}(a) = 1.7143(2.1582 - e^{-0.60222a}) \quad (33)$$

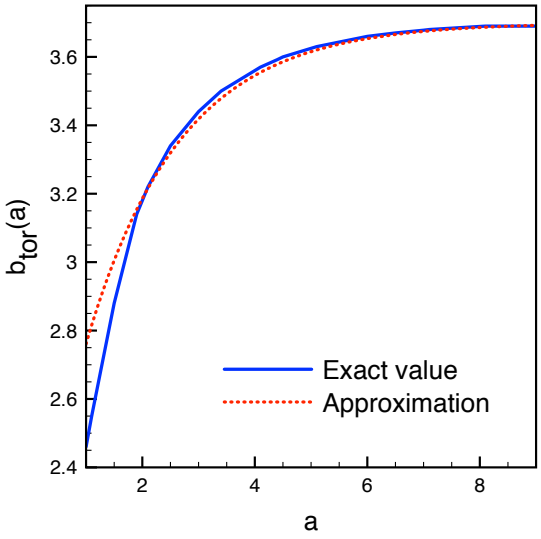

Figure 12: Value of $b_{tor}(a)$, such that the function $1-\exp[-b_{tor}(a)\gamma]$ minimizes the differences with the exact solution for the Side-on emission of a plasma torus with aspect ratio $a = R/r$. As the aspect ratio increases, and the torus becomes two-dimensional, $b_{tor}(a)$ tends to an asymptotic value of ~ 3.7.

With this approximation, the total flux for Side-on emission of a torus is

$$F_{so}(\nu) = (4a + \pi)\frac{r^2}{d^2}S(\nu)\left[1 - e^{-b_{tor}(a)\gamma(\nu)}\right]. \tag{34}$$

An example is shown in figure 13, where the aspect ratio of the torus is $a = 3$.

In this geometry the ratio between the Face-on/Side-on flux for high and low values of $\gamma(\nu)$ is

$$\frac{F_{fo}/F_{so}(a, \gamma(\nu) \to \infty)}{F_{fo}/F_{so}(a, \gamma(\nu) \to 0)} = \frac{b_{tor}(a)}{1.45}. \tag{35}$$

As previously discussed, the higher this ratio, the more sensitive the measurement of opacity of the material. It can be seen from equation 35 that this ratio is highest for a torus with a high aspect ratio, that is, one whose three-dimensional features are least important. The maximum value for the ratio in equation 35 is obtained for the limit $a = R/r \to \infty$, and is ~ 2.5, which is greater than the spherical case, but far from the value for the planar hemi-ellipsoid.

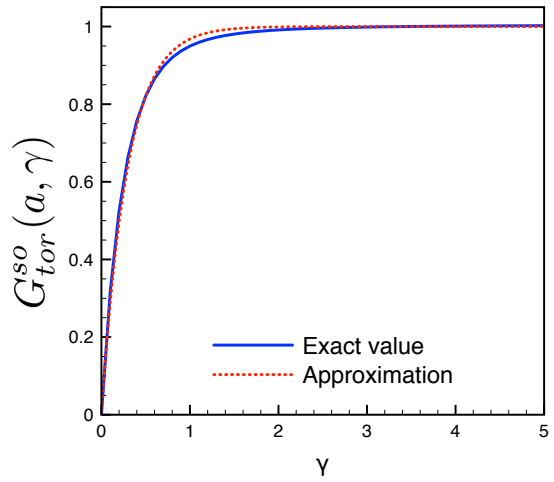

Figure 13: Comparison between the exact value for the Side-on emission of a torus (solid line), given by the integral in equation 31, and the function $1-e^{-b_{tor}(a)\gamma}$ (dashed line). The aspect ratio for this example is $a=3$, and $b_{tor}(3)=3.44$.

7. Summary and conclusions

We have presented expressions for the Face-on and Side-on emission of cylinders, hemi-ellipsoidal shells and toroidal plasmas. Table 1 summarizes the results obtained for the different geometries studied. Note that the parameters a and γ have different definitions depending on the geometry. The functions $b^{fo}_{ell}(a)$, $b^{so}_{ell}(a)$ and $b_{tor}(a)$ are given in equations 20, 25 and 33 respectively. It can be seen how in all cases, the Face-on/Side-on flux ratio can be approximated with a similar functional form. The exact expressions for the Face-on/Side-on flux ratio are given below for comparison.

- Cylinder:

$$\frac{F_{fo}}{F_{so}}(\nu)=2\frac{\left[1-e^{-a\gamma(\nu)}\right]}{\left[1-\frac{\pi}{2}\left(L_{-1}(2\gamma(\nu))-I_1(2\gamma(\nu))\right)\right]} \tag{36}$$

  - Hemispherical shell:

$$\frac{F_{fo}}{F_{so}}(\nu)=2\frac{\left[1-e^{-\gamma(\nu)}(1-\gamma(\nu))-\gamma(\nu)^2E_1(\gamma(\nu))\right]}{\left[1-e^{-2\gamma(\nu)}(1-2\gamma(\nu))-4\gamma(\nu)^2E_1(2\gamma(\nu))\right]} \tag{37}$$

– Hemi-ellipsoidal shell

$$\frac{F_{fo}}{F_{so}}(\nu) = \frac{2}{a} \cdot \frac{G^{fo}_{ell}(a, \gamma(\nu))}{G^{so}_{ell}(a, \gamma(\nu))} \tag{38}$$

– Torus

$$\frac{F_{fo}}{F_{so}}(\nu) = \frac{4\pi a}{4a + \pi} \cdot \frac{\left[1 - \frac{\pi}{2}\left(L_{-1}(2\gamma(\nu)) - I_1(2\gamma(\nu))\right)\right]}{G^{so}_{tor}(a, \gamma(\nu))} \tag{39}$$

In table 1, we show for comparison the exact solution of the Face-on/Side-on ratio compared with the approximations used in this paper. These calculations provide the theoretical basis for using the ratio between the Face-on and the Side-on flux to measure opacity of a plasma of known geometry.

We found that in the cylindrical, hemi-ellipsoidal and toroidal cases, an opacity measurement would be most sensitive to the flux ratio in the limit of a two-dimensional plasma (planar disk, planar hemi-ellipsoid and two-dimensional ring respectively). In particular, we have found that the greatest sensitivity is achieved in the limit of a planar plasma. This is not a surprising result, given that in a planar geometry, the Face-on and Side-on fluxes can be made arbitrarily different depending on the ratio between the plasma height and radius, whereas in the hemi-ellipsoidal case, these fluxes are intrinsically related by the symmetry of the plasma.

8. Acknowledgements

G.P.-C., S. J. R. and J. S. W. gratefully acknowledge support from LLNL under grant number B617350.

References

[1] R. Patch, Simplified method for measuring mean opacities and effective absorption coefficients, J. Quant. Spectrosc. Radiat. Transf. 12 (5) (1972) 969 – 972. doi:https:

Table 1: Summary of the results for the Face-on/Side-on flux ratios obtained for different cases. The functions $b_{ell}^{fo}(a)$, $b_{ell}^{so}(a)$ and $b_{tor}(a)$ are given in equations 20, 25 and 33 respectively. The exact expressions of the Face-on/so ratio for the different geometries are given in equations 37, 38 and 39.

Geometry	Figure	a	γ	Face-on/Side-on flux ratio (approximation)	Plot
Cylinder	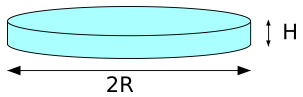	H/R	κR	$\frac{\pi}{2a}\frac{1-e^{-a\gamma}}{1-e^{-1.45\gamma}}$	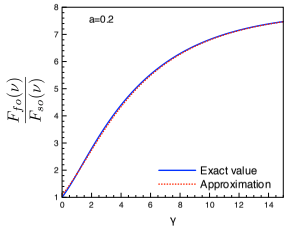
Hemispherical shell	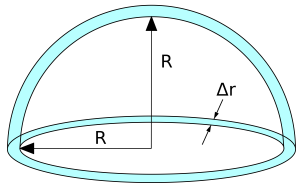	1	$\kappa\Delta r$	$2\frac{1-e^{-1.5\gamma}}{1-e^{-3\gamma}}$	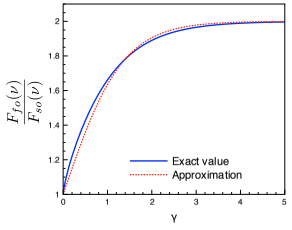
Hemi-ellipsoidal shell	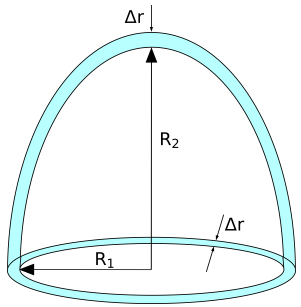	R_2/R_1	$\kappa\Delta r$	$\frac{2}{a}\cdot\frac{1-e^{-b_{ell}^{fo}(a)\gamma}}{1-e^{-2b_{ell}^{so}(a)\gamma}}$	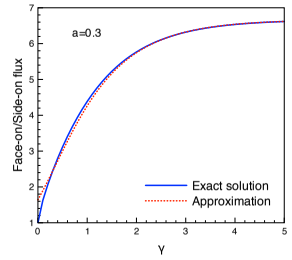
Torus	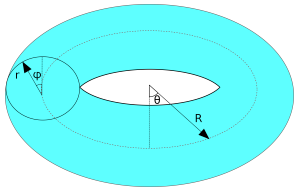	R/r	κr	$\frac{4\pi a}{4a+\pi}\cdot\frac{1-e^{-1.45\gamma}}{1-e^{-b_{tor}(a)\gamma}}$	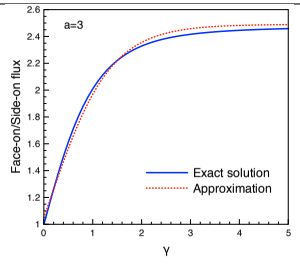

//doi.org/10.1016/0022-4073(72)90084-2.
URL http://www.sciencedirect.com/science/article/pii/0022407372900842

[2] T. R. Preston, S. M. Vinko, O. Ciricosta, P. Hollebon, H.-K. Chung, G. L. Dakovski, J. Krzywinski, M. Minitti, T. Burian, J. Chalupský, V. Hájková, L. Juha, V. Vozda, U. Zastrau, R. W. Lee, J. S. Wark, Measurements of the K-Shell Opacity of a Solid-Density Magnesium Plasma Heated by an X-Ray Free-Electron Laser, Phys. Rev. Lett. 119 (2017) 085001. doi:10.1103/PhysRevLett.119.085001.
URL https://link.aps.org/doi/10.1103/PhysRevLett.119.085001

[3] A. K. Bhatia, S. O. Kastner, The optically thick fe xvii spectrum: X-ray, extreme-ultraviolet, and forbidden line ratios, Astrophys. J. 516 (1) (1999) 482.
URL http://stacks.iop.org/0004-637X/516/i=1/a=482

[4] A. K. Bhatia, J. L. R. Saba, Resonance scattering of fe xvii x-ray and extreme-ultraviolet lines, Astrophys. J. 563 (1) (2001) 434.
URL http://stacks.iop.org/0004-637X/563/i=1/a=434

[5] S. O. Kastner, A. K. Bhatia, Optically thin and thick fe xv spectrum: Effect of self-absorption on the 284.16 resonance line, Astrophys. J. 553 (1) (2001) 421.
URL http://stacks.iop.org/0004-637X/553/i=1/a=421

[6] F. M. Kerr, S. J. Rose, J. S. Wark, F. P. Keenan, Enhancement of optically thick to thin line intensities in solar and stellar coronal plasmas through radiative transfer effects: an angularly resolved study, Astrophys. J. 613 (2004) L181–L184. doi:10.1086/425177.

[7] F. M. Kerr, S. J. Rose, J. S. Wark, An analytic geometry-variant approach to line ratio enhancement above the optically thin limit, Astrophys. J. 629 (2). doi:10.1086/429881.

[8] F. M. Kerr, A. Gouveia, O. Renner, S. J. Rose, H. A. Scott, J. S. Wark, Line radiation effects in laboratory and astrophysical plasmas, J. Quant. Spectrosc. Radiat. Transfer (99) (2006) 363–369. doi:10.1016/j.jqsrt.2005.05.029.

[9] P. Hatfield, Using line intensity ratios to determine the geometry of plasma in stars via their apparent areas, High Energy Density Phys. 6 (3) (2010) 301 – 304. doi:https://doi.org/10.1016/j.hedp.2009.10.001.
URL http://www.sciencedirect.com/science/article/pii/S1574181809000974

[10] D. M. Chambers, P. A. Pinto, J. Hawreliak, I. R. Al'Miev, A. Gouveia, P. Sondhauss, E. Wolfrum, J. S. Wark, S. H. Glenzer, R. W. Lee, P. E. Young, O. Renner, R. S. Marjoribanks, S. Topping, K-shell spectroscopy of an independently diagnosed uniaxially expanding laser-produced aluminum plasma, Phys. Rev. E 66 (2002) 026410. doi:10.1103/PhysRevE.66.026410.
URL https://link.aps.org/doi/10.1103/PhysRevE.66.026410

[11] G. Pérez-Callejo, L. C. Jarrott, D. A. Liedahl, E. V. Marley, G. E. Kemp, R. F. Heeter, J. A. Emig, M. E. Foord, K. Widmann, J. Jaquez, H. Huang, S. J. Rose, J. S. Wark, M. B. Schneider, Laboratory measurements of geometrical effects in the X-ray emission of optically thick lines for ICF diagnostics, Submitted.

[12] R. C. Mancini, J. E. Bailey, J. F. Hawley, T. Kallman, M. Witthoeft, S. J. Rose, H. Takabe, Accretion disk dynamics, photoionized plasmas, and stellar opacities, Phys. Plasmas 16 (4) (2009) 041001. arXiv:https://doi.org/10.1063/1.3101819, doi:10.1063/1.3101819.
URL https://doi.org/10.1063/1.3101819

[13] G. Pérez-Callejo, D. A. Liedahl, M. B. Schneider, S. J.

Rose, J. S. Wark, The use of geometric effects in diagnosing ion density in ICF-related dot spectroscopy experiments, High Energy Density Phys. 30 (2019) 45 – 51. doi:https://doi.org/10.1016/j.hedp.2019.01.005.
URL http://www.sciencedirect.com/science/article/pii/S1574181818301022

[14] M. Abramowitz, I. A. Stegun, Handbook of Mathematical Functions: With Formulas, Graphs, and Mathematical Tables, Applied mathematics series, Dover Publications, 1965.
URL https://books.google.co.uk/books?id=MtU8uP7XMvoC